Photodecaging of a Mitochondria-Localized Iridium(III) Endoperoxide Complex for Two-Photon Photoactivated Therapy under Hypoxia

Shi Kuang, Fangmian Wei, Johannes Karges, Libing Ke, Kai Xiong, Xinxing Liao, Gilles Gas- Ser,, Liangnian Ji, Hui Chao, Gilles Gasser

Photo-Decaging of A Mitochondria-Localized Iridium(III) Endoperoxide Complex for Two-Photon Photoactivated Therapy under Hypoxia

Shi Kuang,[†,#] Fangmian Wei,[†,#] Johannes Karges,[‡] Libing Ke,[†] Kai Xiong,[†] Xinxing Liao,[†] Gilles Gasser,[*,§] Liangnian Ji,[†] and Hui Chao*[,†,⊥]

† MOE Key Laboratory of Bioinorganic and Synthetic Chemistry, School of Chemistry, Guangdong Provincial Key Laboratory of Digestive Cancer Research, The Seventh Affiliated Hospital, Sun Yat-Sen University, Guangzhou, 510006, P. R. China

‡ Department of Chemistry and Biochemistry, University of California, San Diego, 9500 Gilman Drive, La Jolla, CA 92093, United States

§ Chimie ParisTech, PSL University, CNRS, Institute of Chemistry for Life and Health Sciences, Laboratory for Inorganic Chemical Biology, 75005 Paris, France

⊥ MOE Key Laboratory of Theoretical Organic Chemistry and Functional Molecule, School of Chemistry and Chemical Engineering, Hunan University of Science and Technology, Xiangtan, 400201, P. R. China

# These authors contributed equally to this work

KEYWORDS: Bioinorganic Chemistry • Medicinal Inorganic Chemistry • Iridium • Photodynamic Therapy • Photoactivated Chemotherapy

ABSTRACT: Despite the clinical success of photodynamic therapy (PDT), the application of this medical technique is intrinsically limited by the low oxygen concentrations found in cancer tumors which are hampering the production of the therapeutically necessary singlet oxygen ($^1O_2$). To overcome this limitation, we report on a novel mitochondria-localized iridium(III) endoperoxide prodrug (**2-O-IrAn**), which, upon two-photon irradiation in the NIR, synergistically releases a highly cytotoxic iridium(III) complex (**2-IrAn**), singlet oxygen and an alkoxy radical. **2-O-IrAn** was found to be highly (photo-)toxic in hypoxic tumor cells and multicellular tumor spheroids in the nanomolar range. To provide cancer selectivity and improve the pharmacological properties of **2-O-IrAn**, it was encapsulated with a biotin functionalized polymer. The generated nanoparticles were found to nearly fully eradicate the tumor inside a mouse model within a single treatment. This study presents, to the best of our knowledge, the first example of an iridium(III)-based endoperoxide prodrug for synergistic photodynamic therapy/photoactivated chemotherapy, opening up new avenues for the treatment of hypoxic tumors.

Introduction

Photodynamic therapy (PDT) is now used in many countries to treat different medical conditions (e.g., cancer, actinic keratosis). One of the setbacks of this technique is the low concentration of oxygen present in some tissue (e.g.., tumors), avoiding the photosensitizer (PS) to generate singlet oxygen ($^1O_2$) in the event of a type II pathway. There is therefore a need for the development of PSs, which remain phototoxic under hypoxic conditions.[1-7] This is, for example, the basis of photo-activated chemotherapy (PACT).[8-14] Another method to to tackle this drawback is the used of endoperoxides (EPOs) as reversible oxygen traps. Upon light or heat exposure (Scheme 1A), EPOs are able to release the covalently bridged oxygen molecule and generate the therapeutically active singlet oxygen ($^1O_2$).[15-21] While significant research interest has been focused on the development of pyridone EPOs,[22-24] the vast majority of studied compounds for anticancer purposes are based on 9,10-substituted anthracene EPOs.[25-31] Due to the ability of EPOs to deliver the therapeutically necessary oxygen to the target tissue, these compounds could find application for the treatment of hypoxic tumors.

Cyclometalated Ir(III) complexes have been found to be extremely promising photosensitizers (PSs) for photodynamic therapy (PDT) against cancer due to their high biocompatibility, strong luminescence, and high ROS production.[32-37] Based on their overall positive charge and lipophilic nature, such compounds preferably accumulate in the mitochondria.[38-43] As the energetic powerhouse of a cell, the mitochondria in cancer cells are associated with tumorigenesis and tumor progression.[44-48] Tumor cells with low oxygen concentrations adjust their mitochondria metabolism, making these more susceptible to oxidative stress or

reactive species. For this reason, mitochondria present an ideal subcellular location for a PDT agent.[49-53]

The majority of transition metal complexes studied as PDT PSs are excited using UV or visible light.[54-56] As the light penetration depth into the tissue is low at these wavelengths, the application of such compounds is limited to superficial lesions or small tumors.[57-59] To overcome these limitations, noticeable attention has been devoted towards the development of two-photon absorbing chromophores. In such a process, the compounds absorb simultaneously two photons of low energy/long wavelength, allowing for excitation in the biological spectral window (700-1000 nm). Besides deeper light tissue penetration depth, two-photon excitations are also associated with a higher spatial and temporal resolution, presenting this technique as a promising alternative.[60-63] Previous studies by our group have reported on the use of an Ir(III) anthraquinone complex which is able to

Scheme 1. A) Previously reported EPO photosensitizers, B) Previously reported carbon radical photosensitizers, C/D) Schematic illustration of the mechanism of action of the Ir(III) complex by photodynamic therapy/photoactivated chemotherapy.

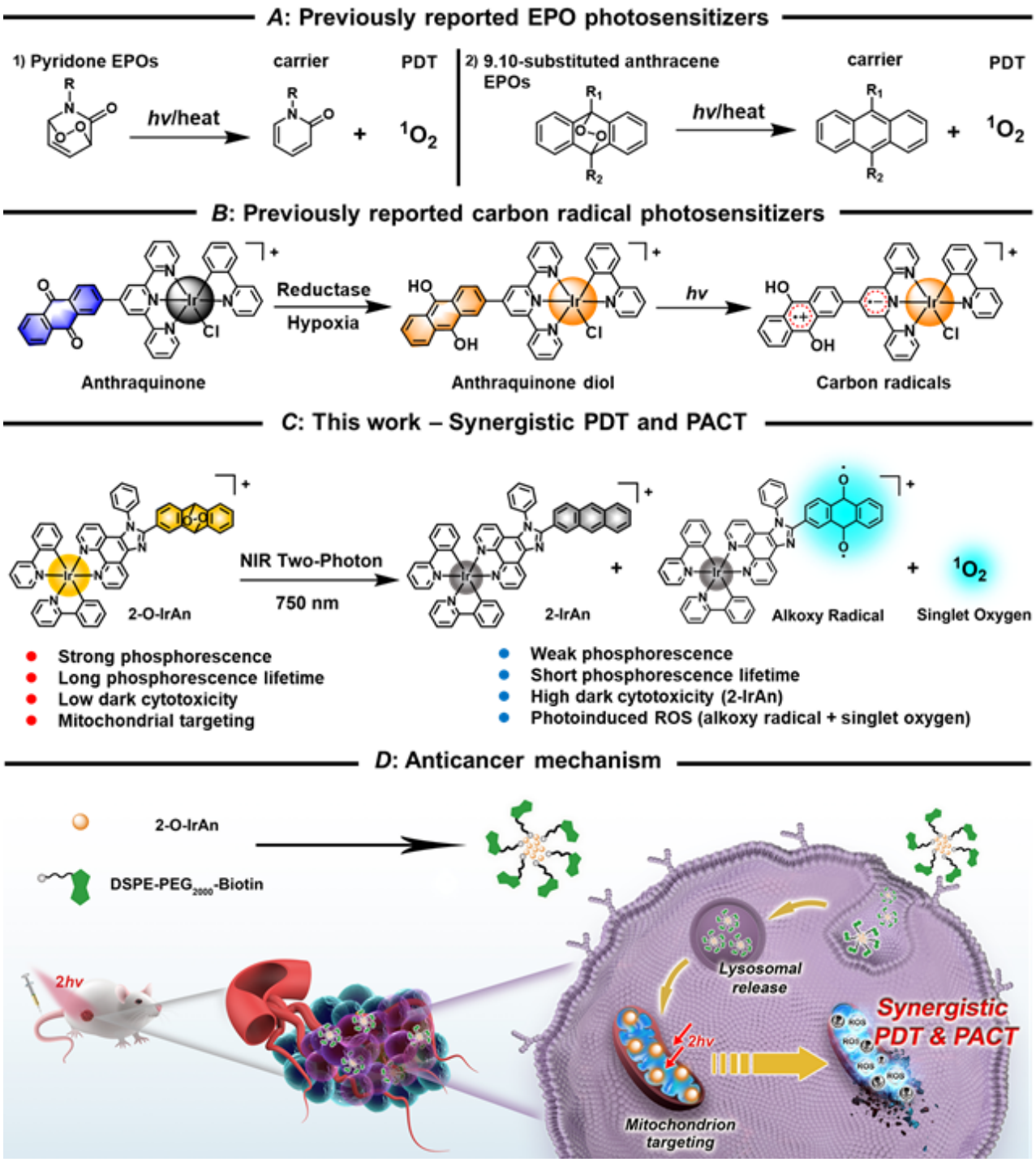

generate carbon radicals under hypoxic conditions (Scheme 1B). Despite its activity under hypoxic conditions, the metal complex was found to have a phototoxic effect in the micromolar range.[38] To provide a potential application in a clinical setting, compounds with a higher potency are required. Based on drawbacks to overcome and these previous studies, in this article, we report on a novel cyclometalated Ir(III) EPO complex as a light-activated prodrug. Upon light irradiation, the metal complex synergistically releases a highly cytotoxic iridium(III) complex, $^1O_2$ and an alkoxy radical (Scheme 1C).[67] Thanks to a mechanism independent of the presence of oxygen, the lead compound of this study, namely **2-O-IrAn,** was found to have a phototoxicity upon one- or two-photon irradiation in the nanomolar range in hypoxic adenocarcinomic human alveolar basal epithelial cells as well as multicellular tumor spheroids. Insights into the biological mechanism revealed that the metal complex primarily accumulates in the mitochondria, where it causes cellular damage through loss of the mitochondrial membrane potential and ultimately triggers cell death by apoptosis. To provide cancer selectivity as well as improve the pharmacological properties of **2-O-IrAn**, it was encapsulated into a biotin functionalized phospholipid (Scheme 1D). Upon intravenous injection, the generated nanoparticles were able to drastically reduce the tumor volume in tumor-bearing mice upon two-photon irradiation in the NIR. Overall, this study reports one of the most efficient metal-based PDT PSs working under hypoxic conditions and that can be excited with 2P.

Results

Synthesis and Characterization. Previous studies on EPOs have shown that the position of functionalization on the anthracene moiety has a significant influence on the efficiency of the peroxidation reaction, endoperoxide stability, and cytotoxicity.[25-31] As the privileged location for a photorelease mechanism, the anthracene moiety was covalently linked in 2- or 9-position to the Ir(III) complex. The corresponding metal complexes are referred to as **2-IrAn** and **9-IrAn**, respectively and the endoperoxide versions as **2-O-IrAn** and **9-O-IrAn**, respectively. The ligand scaffold was synthesized by a condensation reaction of 1,10-phenanthroline-5,6-dione with the corresponding anthracene functionalized aldehyde in the presence of ammonium acetate. The generated ligand was then coordinated to the metal center of $[Ir(2\text{-phenylpyridine})_2Cl]_2$ upon release of the chloride ions to generate **2-IrAn** and **9-IrAn** (Scheme S1). The compounds were characterized by ^{1}H- and ^{13}C-NMR spectroscopy and mass spectrometry (Figure S1-S4) and their purity checked by HPLC as well as elemental analysis.

Photophysical Properties. With the compounds in hand, their ability to act a PSs under normoxic conditions was investigated upon exposure of solutions of the metal complexes to a LED light source (405 nm, 20 mW/cm^2) and monitoring of changes in the molecular structure by mass spectrometry. At the start of the experiment, the compounds **2-IrAn** and **9-IrAn** showed a single mass peak, corresponding to the intact metal complex. Upon irradiation of a solution of the compound, the mass peak of the metal complex (m/z = 973.6) decreased while a peak at higher molecular weights (m/z = 1005.5), corresponding to a single oxygen molecule bound to the compound, increased independence of the exposed irradiation time (Figure S7-S8). Using high-resolution mass spectrometry, the identity of the endoperoxide functionalized complexes **2-O-IrAn** and **9-O-IrAn** was verified (Figure S9-S10). A tandem mass spectrometric analysis revealed the presence of several oxygen-containing intermediates (Figure S11-S12). For a deeper insight into the photophysical mechanism, solutions of **2-IrAn** and **9-IrAn** were irradiated under normoxic conditions at 405 nm and changes in their molecular structure were monitored by ^{1}H- and ^{13}C-NMR spectroscopy. Following this, the solutions were degassed and irradiated under an argon atmosphere as a model for the hypoxic conditions found in cancerous cells. Upon light exposure in normoxia, the ^{1}H NMR spectrum of **2-IrAn** showed a doubled signal set of peaks corresponding to the anthracene moiety (Figure S13). A similar effect was observed in the ^{13}C NMR spectrum as well as the presence of a distinctive peak at ~182 ppm corresponding to the carbon-oxygen bond (Figure S14). These results suggest that the $^1O_2$ is covalently attached to the anthracene fraction of the molecule. Solutions of the generated oxygen trapped endoperoxide complexes **2-O-IrAn** and **9-O-IrAn** in DMSO were degassed with argon to generate an hypoxic environment. Afterwards, the solutions were exposed to light (405 nm). As expected, a decrease of the previously reported peaks was observed (Figure S13-S14), indicating the release of $^1O_2$ and the regeneration of **2-IrAn**. Using an analogous experimental procedure, the photophysical effects of **9-IrAn** were studied. While changes in the ^{1}H NMR and ^{13}C NMR spectra similar to the ones for **2-IrAn** were observed, only a small fraction of the sample was found to be converted into the endoperoxide functionalized compound (Figure S15-S16). These results indicate the superior properties of **2-IrAn** to act as a PS in comparison to **9-IrAn**. Capitalising on this, the endoperoxide complexes **2-O-IrAn** and **9-O-IrAn** were intentionally prepared by photo-induced self-catalysis using a 405 nm light source (Scheme S2). The obtained ^{1}H NMR spectrum for **2-O-IrAn** (Figure S5) was found to be in agreement with a solution of **2-IrAn** exposed to light under normoxic conditions. The peroxidation and the photo-decaging reaction of the metal complexes **2-O-IrAn** and **9-O-IrAn** were further investigated upon monitoring of the emission profile of the respective compound. Interestingly, while **2-IrAn** and **9-IrAn** were found to be poorly emissive, the corresponding endoperoxide complexes **2-O-IrAn** and **9-O-IrAn** generated during light irradiation are much more luminescent. Therefore, the generation of the EPOs was followed by monitoring of the emission with differnt irradiation time under normoxic and hypoxic conditions. Within 10 min, the asymptotic maximum of the conversion was reached with an 84-times stronger luminescence for **2-O-IrAn** and an 18-times stronger luminescence for **9-O-IrAn** in comparison to their respective complexes (Figure 1A, Figure S17, Video S1). Following this, the ability of the endoperoxide complexes **2-O-IrAn** and **9-O-IrAn** to release $^1O_2$ under hypoxic conditions was studied by monitoring analogously the emission profile of the compound. While the emission spectrum of **2-O-IrAn** reached the asymptotic minimum

after 2 min of irradiation with approximately 80% of photo-decaged compound, (Figure 1B), **9-O-IrAn** reached its asymptotic minimum already after 30 s of irradiation with approximately 20% of photo-decaged product (Figure S17). In addition, measurements of the excited state lifetime under hypoxic conditions revealed that the endoperoxide complexes **2-O-IrAn** (874 ns) and **9-O-IrAn** (630 ns) have longer lifetimes than **2-IrAn** (365 ns) and **9-Ir-An** (452 ns), respectively (Table S1). For a quantitive assessment, the reaction rates of the peroxidation and photo-decaging reactions were determined by monitoring of characteristic peaks in the absorption spectra of the corresponding compound. In agreement with previous observations, **2-IrAn** was found to have a faster reaction rate for the peroxidation reaction ($k = 0.216\ min^{-1}$) as well as photo-decaging reaction ($k = 0.0245\ s^{-1}$) in comparison to **9-IrAn** (Figure 1C-D, Figure S19-S20). In addition, the photophysical reactivity of the metal complexes was studied by HPLC-MS analysis. While **2-IrAn** has a retention time of 15.1 min, the endoperoxide analogous compound **2-O-IrAn** is associated with a higher polarity. Therefore, the peak was observed at a reduced retention time (13.8 min). In agreement with the previous investigations, ~80% of **2-IrAn** was found to be converted

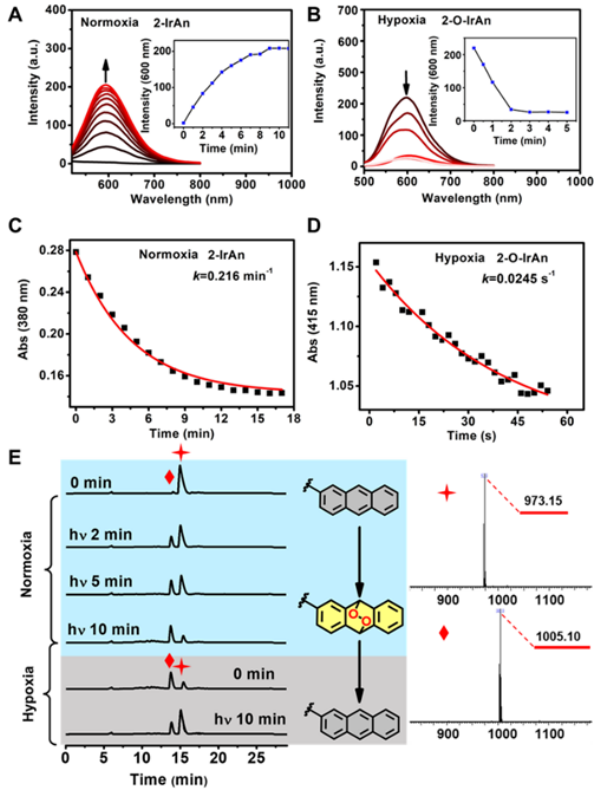

Figure 1. Kinetic of the photoinduced peroxidation reaction under normoxic conditions of **2-IrAn** (2 μM) and the photoinduced decaging reaction under hypoxic conditions of **2-O-IrAn** (2 μM) upon irradiation at 405 nm (20 mW/cm^2). (A/B) Monitoring of the emission profile. (C/D) Monitoring of a characteristic absorption peak for determination of the reaction rate. (E) Monitoring of the conversion by HPLC-MS.

to **2-O-IrAn** under normoxic conditions upon irradiation for 10 min. Upon irradiation of this solution under hypoxic conditions, the majority of the compound is converted back to **2-IrAn**. The direct comparison between **2-IrAn** and **9-IrAn** shows the higher peroxidation and photo-decaging reaction efficiency of **2-IrAn** (Figure 1E, Figure S21).

Besides the released $^1O_2$ upon irradiation, the ability to generate $^1O_2$ from molecular oxygen ($^3O_2$) under normoxic conditions was evaluated using the non-fluorescent dichlorodihydrofluorescein diacetate probe which is converted in the presence of ROS into the highly fluorescent dichlorofluorescein. **2-O-IrAn** ($\Phi = 0.79$) was found to have a very high singlet oxygen quantum yield in comparison to **9-O-IrAn** ($\Phi = 0.16$) (Figure S22). The ability to produce ROS was further investigated under hypoxic conditions. While no ROS generation was observed for the complexes in the dark, a significant production was observed upon irradiation for all compounds. The direct comparison showed that the endoperoxides complexes **2-O-IrAn** and **9-O-IrAn** were able to produce ROS more efficiently than **2-IrAn** and **9-IrAn**. Overall, **2-O-IrAn** was identified with the strongest ROS production among these compounds under hypoxic conditions (Figure S23). For identification of the type of ROS generated upon irradiation under hypoxic conditions, electron spin resonance (ESR) spectroscopy was employed using the oxygen radical scavenger 5,5-dimethyl-1-pyrroline *N*-oxide or the $^1O_2$ scavenger 2,2,6,6-tetramethylpiperidine. As expected from our previous results presented above, all compounds were found to produce $^1O_2$, as indicated by the characteristic triplet signal observed (Figure S24). Interestingly, the incubation of **2-O-IrAn** with 5,5-dimethyl-1-pyrroline *N*-oxide (DMPO) in 1,4-dioxane under hypoxic conditions and upon light exposure showed a distinctive set of signals which are corresponding to the presence of an alkoxy radical (Figure S25) [68] which is likely generated by the peroxy bond cleavage reaction.[15] However, upon incubation in phosphate-buffered saline, the generation of hydroxy radicals by a type I pathway was observed (Figure S25). For verification of the species generated upon incubation of **2-O-IrAn** with DMPO and exposure to light under hypoxic conditions, tandem mass spectrometry was utilized. The spectrum (Figure S26) showed a peak corresponding to the DMPO-adduct (m/z = 1116) as well as the formation of an alkoxy radical species (m/z = 1004). Alkoxy radicals have been previously reported with a cytotoxic effect.[69] Overall, these results indicate that **2-O-IrAn** is able to interact in a hypoxic environment upon irradiation by a multitude of mechanism of action by production of $^1O_2$ as well as an alkoxy radical. To evaluate whether these compounds could be excited by a two-photon light source, the two-photon absorption cross sections (GM = Göppert-Mayer, 1 GM = 1 × 10^{-50}·cm^4·s^{-1}·photon^{-1}) in methanol were determined. **9-O-IrAn** (245 GM) and **2-O-IrAn** (297 GM) were found with strong two-photon absorption at 750 nm (Table S1). Due to the superior photophysical properties (i.e., stronger luminescence, higher singlet oxygen production and faster release of oxygen upon irradiation), following research efforts have been focused on the **2-IrAn/2-O-IrAn** pair.

Table 1. (Photo)cytotoxicity of the metal complexes (μM) towards A549 cells

Oxygen condition	hypoxic conditions (1% O_2)			normoxic conditions (21% O_2)		
Complexes(μM)	2-IrAn	2-O-IrAn	cisplatin	2-IrAn	2-O-IrAn	cisplatin
Dark	0.85±0.87	41.42±1.10	20.93±0.76	0.83 ± 0.76	49.42 ± 0.92	24.61 ± 0.86
Light[a]	0.72±0.68	0.06 ±1.80	21.49±1.41	< 0.026 ± 0.001	< 0.052 ± 0.001	24.74 ± 0.80
PI[b]	1.2	690.3	1.0	>31.5	>959.1	1.0

[a] Irradiated at 405 nm by LED light (20 mW/cm^2) for 10 min. [b] PI (photocytotoxicity index) is the ratio of dark-to-light toxicity and corresponds to the efficiency of the light treatment.

The stability of a compound is a crucial parameter for its use in a biological setting. For this purpose, **2-O-IrAn** was incubated in phosphate-buffered saline for various incubation times up to 24 h and then analyzed by HPLC. Promisingly, the chromatograms and MS did not show any changes, indicative of the stability of the compound in a biological environment (Figure S27).

(Photo)cytotoxicity Studies. Based on these promising properties, the cellular effects of the **2-IrAn/2-O-IrAn** pair were investigated. The cytotoxic effect caused by the metal complexes was studied in the dark or upon irradiation at 405 nm (higher wavelength not possible with one photon – no absorption is observed above this wavelength) in a 3-(4,5-dimethylthiazol-2-yl)-2,5-diphenyltetrazolium romide (MTT)-based assay towards adenocarcinomic human alveolar basal epithelial (A549) cells under normoxic (21% O_2) and hypoxic conditions (1% O_2). While **2-O-IrAn** was found to be slightly cytotoxic in the dark (IC_{50}=41.42-49.4 μM), the **2-IrAn** complex generated upon release of oxygen was found to be highly cytotoxic (IC_{50}=0.83-0.85 μM) in a normoxic and hypoxic environment. Upon light exposure, **2-IrAn** generated ROS and caused a phototoxic effect in the low nanomolar range in a normoxic environment ($IC_{50,405nm}$ < 26.32 nM, PI>31.5) but loses its therapeutic effect under hypoxic conditions. In contrast, **2-O-IrAn** was found to have an excellent therapeutic efficiency with a phototoxic effect in the low nanomolar range under normoxic conditions ($IC_{50,405nm}$ < 51.53 nM, PI > 959.1) and remained highly (photo-)toxic under hypoxic conditions ($IC_{50,405nm}$ = 60 nM, PI = 690.3) (Table 1). These results are promising since most PDT agents show a highly reduced therapeutic effect under hypoxic conditions. The difference in therapeutic efficiency towards traditional PSs is presumably attributed to the multiaction mechanism of **2-O-IrAn** through the release of a highly cytotoxic iridium(III) complex and singlet oxygen as well as the generation of an alkoxy radical upon irradiation.

ROS Generation under Hypoxia and Biodistribution. Encouraged by these preliminary results, research efforts have been devoted towards unveiling the underlying biological mechanism of action. For verification of the ability of **2-O-IrAn** to generate ROS under hypoxic conditions, A549 cells were incubated with the ROS probe dichlorodihydrofluorescein diacetate and exposed to light irradiation. The production of the bright green fluorescent dichlorofluorescein in the presence of ROS was time-dependently monitored by laser scanning confocal microscopy. As expected, immediately after light irradiation, a strong fluorescence signal was detected, indicating the ability of **2-IrAn** and **2-O-IrAn** to produce ROS under hypoxic conditions in a cellular environment (Figure S28).

Meanwhile, a rupture of the cell membrane and vesicles formation within the cell can be also observed, which further indicates the irreversible state of cell death. Upon utilizing the luminescence properties of **2-O-IrAn**, the subcellular localization was studied by laser scanning confocal microscopy by comparison of the distribution pattern obtained from the compound with cell organelle-specific dyes. The co-incubation of the metal complex with Mito-Tracker Deep Red demonstrated an excellent congruency (PCC = 0.96), indicative of the accumulation of **2-O-IrAn** primarily in the mitochondria (Figure 2A). As a complementary technique, the subcellular localization of the compound was studied upon extraction of the several key organelles (i.e., mitochondria, lysosome, cytoplasm, nucleus) and determination of the Ir content inside these by inductively coupled plasma mass spectrometry (ICP-MS). Upon incubation of **2-O-IrAn** for 4 h, approximately 42.7 fg/cell were found to be internalized. In agreement with the assessment by laser scanning confocal microscopy, 74% of the iridium content was found inside the mitochondria, confirming this organelle as the primary target of the metal complex (Figure 2B). Notably, the high accumulation inside a single vital organelle and in particular the mitochondria, which is highly susceptible to oxidative stress in cancerous cells, is considered advantageous for a therapeutic agent. Interestingly, **2-IrAn** was found to have a higher cellular uptake than **2-O-IrAn** (Figure S29), which might contribute to the higher dark cytotoxicity of **2-IrAn**. As a simplified model for cellular uptake, the partition coefficient between octanol and water of the metal complexes was determined. In agreement with the cellular uptake, **2-O-IrAn** (log*P* = 0.472) was found to be significantly more hydrophilic than **2-IrAn** (log*P* = 0.969) (Figure S30).

Phosphorescence Lifetime Imaging. Based on the previous observation that the endoperoxide complex **2-O-IrAn** is significantly longer-lived than **2-IrAn**, their conversion within cancerous cells under hypoxic conditions was monitored using phosphorescence lifetime imaging microscopy (PLIM). This technique provides high selectivity and spatial resolution of the respective species.[67, 68] Indeed, upon irradiation for 9 min, a shift of the phosphorescence lifetime distribution from ~840 ns

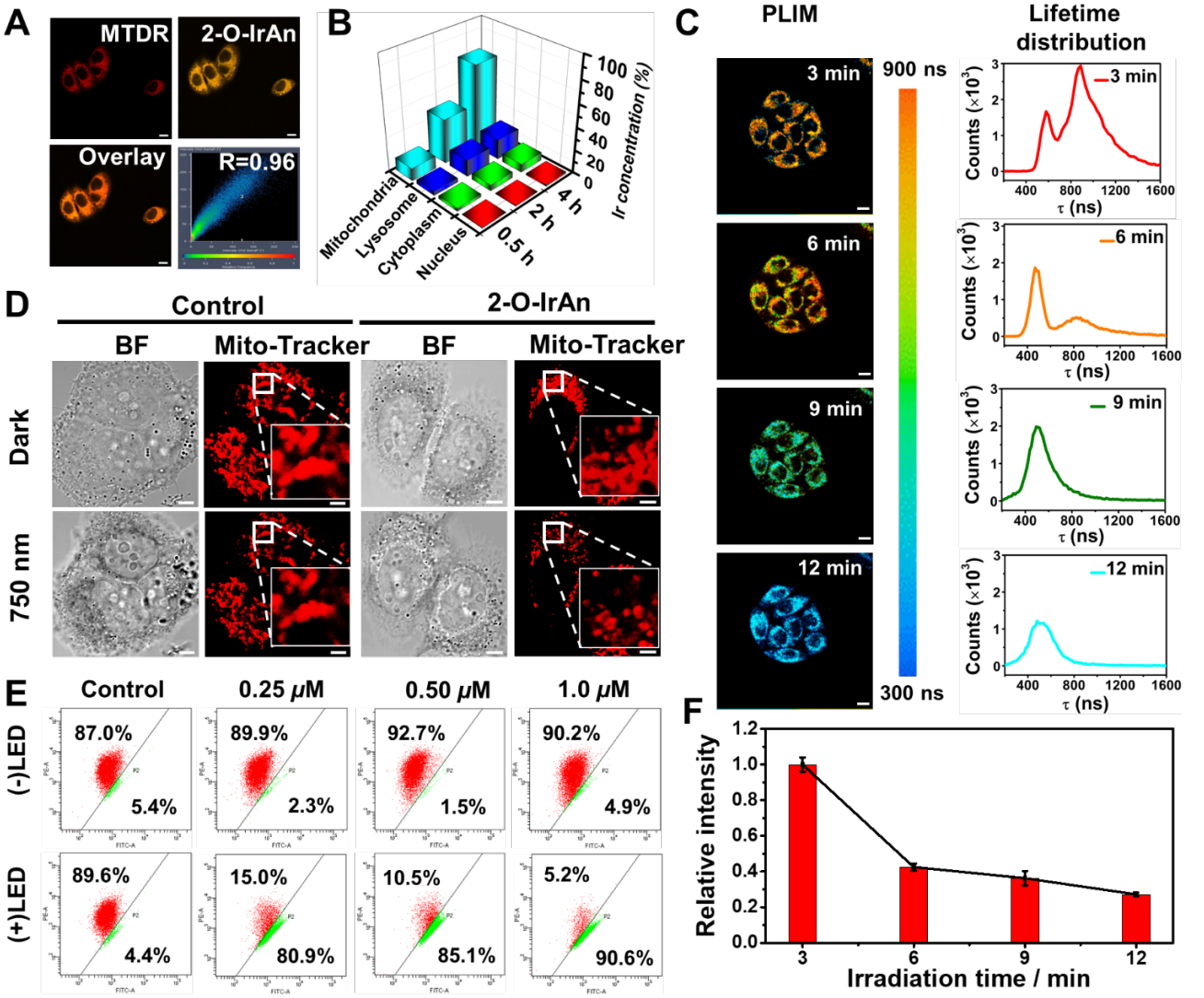

Figure 2. A) Confocal microscopy images of A549 cells upon incubation with **2-O-IrAn** (2 μM) of 4 h, followed incubation with Mito-Tracker Deep Red (MTDR, 50 nM). Top left to right: MTDR ($\lambda_{ex/em}$ = 633/656 ± 10 nm), **2-O-IrAn** ($\lambda_{ex/em}$ = 405/600 ± 20 nm); bottom left to right: Overlay and Pearson Colocation coefficient of MTDR and **2-O-IrAn**; Scale bar: 10 μm. B) Time-dependent subcellular distribution of **2-O-IrAn** in the mitochondria, lysosomes, cytoplasm, and nucleus determined by ICP-MS. C) Left from top to bottom: PLIM images of A549 cells upon incubation with **2-O-IrAn** (2 μM) and two-photon irradiation at 750 nm under hypoxic conditions. Right: Lifetime distribution of the emission corresponding to the PLIM; Scale bar: 10 μm. D) Confocal microscopy images of morphological changes of A549 cells upon incubation with **2-O-IrAn** (2 μM) and two-photon irradiation at 750 nm under hypoxic conditions. Scale bar: 5 μm. E) Plot of the flow cytometry result upon incubation with JC-1 as a mitochondrial membrane potential probe upon incubation with **2-O-IrAn** and 405 nm (20 mW/cm²) light irradiation under hypoxic conditions. F) Changes in phosphorescence intensity in correlation of the irradiation time.

to ~520 ns within a hypoxic environment was observed (Figure 2C). Besides the decrease in lifetime, a reduced emission signal within the cells was observed (Figure 2F). This finding is in agreement with the previous observation that **2-IrAn** is poorly emissive. These combined results suggest the release of ROS and the conversion of **2-O-IrAn** to **2-IrAn** within hypoxic cancerous cells. Microscopy images further showed significant signs for cellular damage including mitochondria shrinkage and vesicles formation within the cell (Figure 2D and S28).

Cell Death Mechanism. the cell membrane integrity upon treatment with **2-O-IrAn** was studied using lactic dehydrogenase as a reporter. Even at low concentrations of 0.5 μM, a significant increase in lactic dehydrogenase content inside the cell media was observed, suggesting the rupture of the cell membrane and leakage of the cellular content (Figure S31). Followingly, the cell death mechanism of **2-IrAn** and **2-O-IrAn** was studied by measuring the cell viability upon preincubation with apoptosis (Z-VAD-FMK), paraptosis (cycloheximide), lysosomal pathway (leupeptin), autophagy (3-methyladenine) or necrosis (necrostatin-1) inhibitors. Since the incubation with Z-VAD-FMK increased both cell survival while necrostatin-1 only work for **2-IrAn** group, an apoptotic cell death mechanism for **2-O-IrAn** and **2-IrAn**, and necrosis for **2-IrAn** are indicated (Figure S32). As a complementary method, the cell death mechanism was studied using the Annexin-V/Propidium iodide pair. While upon treatment of A549 cells with **2-O-IrAn** no

cell death in the dark was observed, a significant amount of early and late apoptotic cells were detected in a concentration-dependent manner (Figure S33). Based on the primary accumulation of **2-O-IrAn** in the mitochondria, the effects of this compound on the mitochondrial membrane potential (MMP) was investigated using the JC-1 reporter molecule. Upon treatment of A549 cells with **2-O-IrAn** in the dark, a red fluorescence signal corresponding to JC-1 in its aggregated state was observed, suggestive of the intactness of the MMP. On the contrary, upon light exposure, a strong green fluorescence signal was detected which corresponds to the conversion of JC-1 into its monomeric form and therefore the loss of the MMP. Interestingly, even at treatments at very low concentrations of 0.25 μM, more than 80% of the MMP was lost (Figure 2E).

3D multicellular tumor spheroids. Following the evaluation in a 2D monolayer model, the biological effects of **2-O-IrAn** were studied in 3D multicellular tumor spheroids (MCTS). MCTS are a tissue model which more realistic mimics proliferation gradients, cellular heterogeneity as well as hypoxia within their center. To investigate whether the

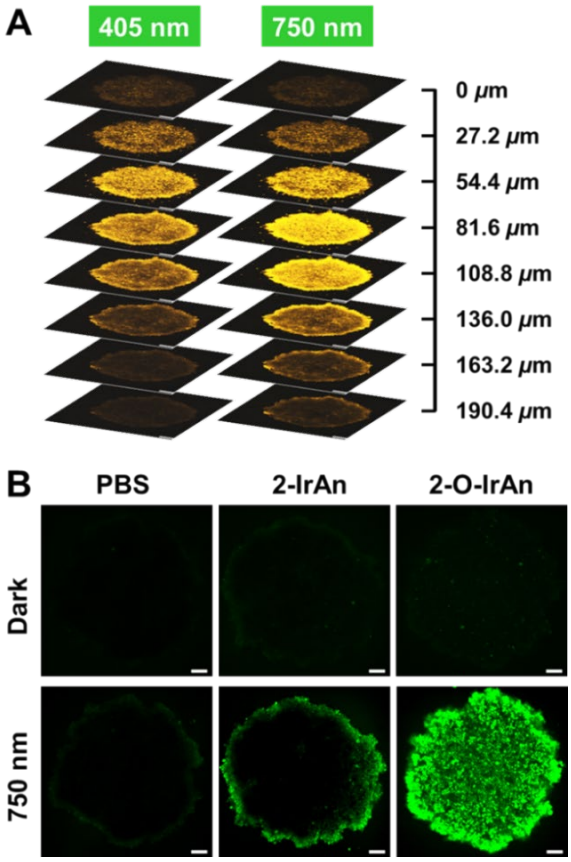

Figure 3. A) Z-stack confocal microscopy images of an A549 MTCS upon incubation with **2-O-IrAn** (2 μM) and exposure to one- (405 nm) or two-photon (750 nm) light. B) Representative image a A549 MCTS upon incubation with **2-O-IrAn** (2 μM) and the ROS probe dichlorodihydrofluorescein diacetate (500 nM) and exposure to two-photon (750 nm) light. Detection of dichlorodihydrofluorescein: $\lambda_{ex/em}$ = 488/530 ± 20 nm, Scale bar: 100 μm.

compounds are able to penetrate the 3D cellular architecture, Z-stack laser scanning confocal microscopy was used. Beside an excitation with a one-photon light source, the metal complex was also exposed to two-photon light. Two-photon excitation is associated with a high spatial and temporal resolution as well as deeper tissue penetration depth.

Importantly, the A549 MCTS showed a strong luminescence signal for **2-O-IrAn** at every section depth with both light sources, indicative of the ability of the metal complexes to fully penetrate the 3D cellular architecture (Figure 3A). For verification of the ability of the metal complex to generate ROS, A549 MCTS were incubated with the compound, the ROS probe dichlorodihydrofluorescein diacetate and exposed to two-photon irradiation. Notably, previous studies have shown that the outer sphere of MCTS has normal levels of oxygen contrary to the center, in which a hypoxic environment is established. While the treatment with **2-IrAn** showed only at the outer sphere of the MCTS the green fluorescence of dichlorofluorescein, every section of the MCTS was green emissive upon treatment with **2-O-IrAn**. This observation indicates the ability of **2-O-IrAn** to generate the therapeutic species within 3D cellular architecture at various oxygen levels, including a hypoxic environment (Figure 3B). Capitalizing on these encouraging results, the (photo-)toxic effect in A549 MCTS was quantified upon measurement of their relative ATP concentration. While **2-IrAn** was found to have significant dark toxicity (IC_{50} = 7.47μM), no additional effect upon light exposure was observed. On the contrary, **2-O-IrAn** had only a slight cytotoxic effect in the dark (IC_{50} = 88.1 μM) and excellent phototoxicity (IC_{50} = 0.73 μM, PI = 120.7) upon exposure to two-photon irradiation at 750 nm (Table S2). For verification of the cellular damage caused by the compounds, MCTSs were treated in the dark or upon irradiation with the compound (2 μM) and cell viability was assessed with a cell live/dead stain. In agreement with our previous observations, a mixture of living and dead cells was observed upon treatment with **2-IrAn** in the dark or upon light irradiation. In contrast, no cell damage was observed upon treatment in the dark with **2-O-IrAn**. However, upon two-photon irradiation, nearly all cells within the MCTS were eradicated, confirming the efficiency of the treatment at every section depth (Figure S34).

DSPE-PEG-Biotin Encapsulation. The metal complex **2-O-IrAn** was encapsulated with the **DSPE-PEG** polymer to form the nanoformulation **DSPE-PEG-Biotin@2-O-IrAn**. Previous studies have shown that phospholipids are able to (1) improve water solubility, (2) improve blood circulation half-life time, (3) provide tumor-targeting through the over-expressing of the sodium multivitamin transporter, which is primarily responsible for the uptake of biotin, and (4) reduce cytotoxicity and side effects.[69-71] Using dynamic light scattering, the hydrodynamic diameter of the nanoparticles was determined to be on average 116 nm, which is considered optimal for drug delivery purposes (Figure S35).

To ensure that the encapsulation did not profoundly influence the photophysical properties and, significantly, the ability to generate therapeutically necessary ROS, **DSPE-PEG-Biotin@2-O-IrAn** was incubated with dichlorodihydrofluorescein diacetate under hypoxic conditions and exposed to light. A strong green fluorescence signal for dichlorofluorescein was observed, suggesting ROS's efficient production (Figure S36). As the vast majority of nanoparticles are taken up into the cells by an endocytotic

mechanism, their stability within the lysosomal acidic environment needed to be investigated. For this purpose, **DSPE-PEG-Biotin@2-O-IrAn** was incubated in an aqueous solution at physiological (pH = 7.4) or acidic (pH = 5.0) conditions and the stability of the particles was monitored by transmission electron microscopy. While no changes in size or morphology for the nanoparticles under physiological conditions were noticed, degradation was observed at acidic pH. After 2 h, a significant amount of the nanoparticles showed release of their load and within 6 h the whole sample did not show any intact particles (Figure S37). After the encapsulation, **DSPE-PEG-Biotin@2-O-IrAn** remains highly phototoxicity towards hypoxic A549 cells as well as A549 MCTSs (Figure S38). Followingly, the ability of **DSPE-PEG-Biotin@2-O-IrAn** to be internalized into the cancerous cells and its subcellular localization was studied by laser scanning confocal microscopy time-dependently. With the prolongation of the incubation time, the emission intensity within the cells was steadily increasing, indicative of the effective cellular uptake of the nanoparticles. Interestingly, **DSPE-PEG-Biotin@2-O-IrAn** initially showed a high colocalization coefficient with the lysosomes of 0.73 which gradually decreased to 0.54. In the meantime, the colocalization coefficients for the mitochondria strongly increased from 0.37 to 0.85. These results suggest that **DSPE-PEG-Biotin@2-O-IrAn** is

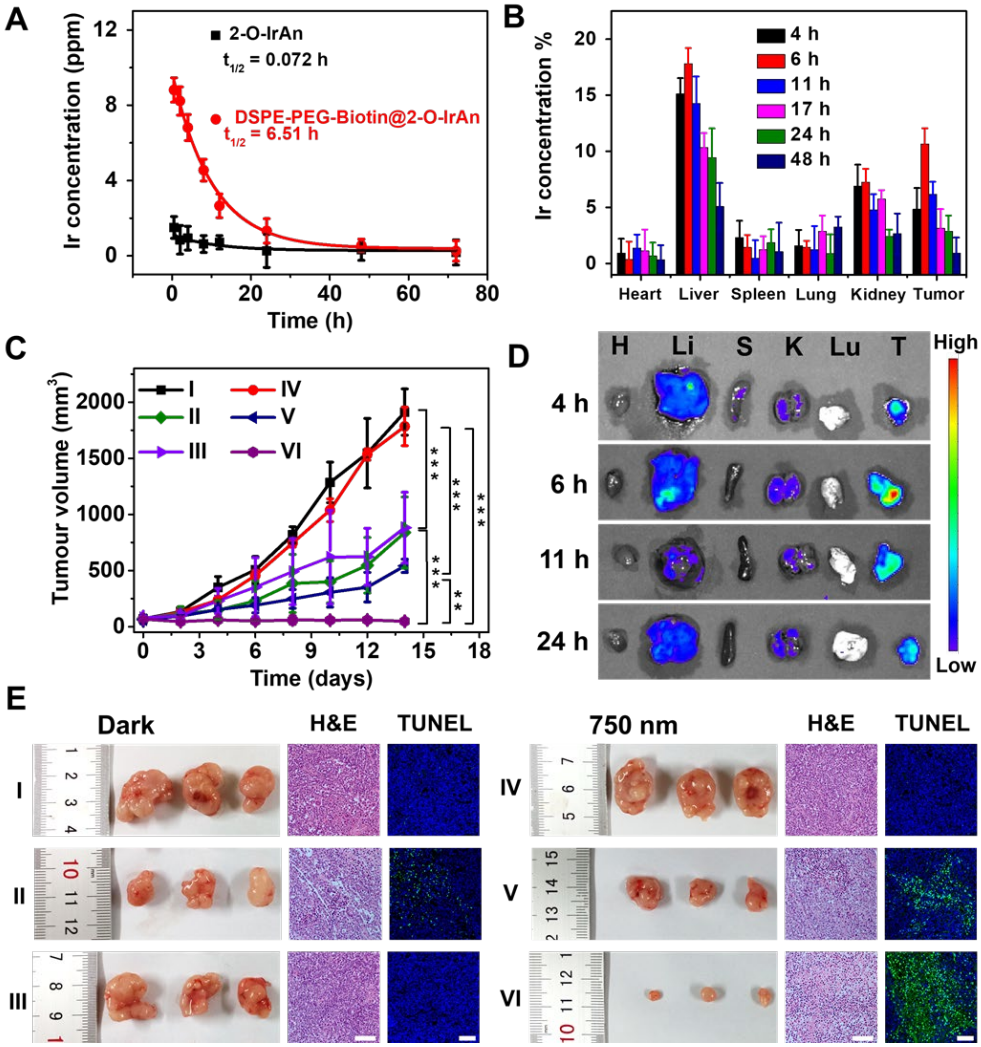

Figure 4. A). Concentration of Ir in the mice blood after intravenous injection of **2-O-IrAn** (1.0 mg/mL) or **DSPE-PEG-Biotine@2-O-IrAn** (1.0 mg/mL). Biodistribution of **DSPE-PEG-Biotine@2-O-IrAn** at various time points in the major organs (from left to right: heart, liver, spleen, kidney, lung) determined by ICP-MS (B) and *in vivo* imaging system (D). C) Tumor growth inhibition curves after the respective treatment. E) Representative pictures of the tumor after the respective treatment and Hematoxylin-Eosin (H&E) stain (Scale bar: 200 μm)and TUNEL stain (Scale bar: 100 μm) of the tumor tissue after the respective treatment. I: physiological saline (200 μL); II: cisplatin (4 mg/kg, 200 μL); III: **DSPE-PEG-Biotine@2-O-IrAn** (1.0 mg/kg, 200 μL); IV: physiological saline (200 μL) + two-photon irradiation (750 nm, 50 mW, 300 s); V: cisplatin (4 mg/kg, 200 μL) + two-photon irradiation (750 nm, 50 mW, 300 s); VI: **DSPE-PEG-Biotine@2-O-IrAn** (1.0 mg/kg, 200 μL) + two-photon irradiation (750 nm, 50 mW, 300 s). (**P<0.01, *** p<0.001)

internalized by an endocytotic mechanism and primarily localized in the lysosomes before being released of the acidic lysosomes environment. The Ir(III) complex then accumulates in the mitochondria (Figure S39).

***In Vivo* Biodistribution Studies.** Encouraged by these promising results, the therapeutic properties were further investigated upon intravenous injection into A549 tumor-bearing Nu/Nu mice. While **2-O-IrAn** was found to be

directly filtered out of the bloodstream with a blood circulation half-life time of approximately 4.3 min, **DSPE-PEG-Biotin@2-O-IrAn** remained significantly longer in the blood stream with a blood circulation half-life time of 6.5 h. This clearly shows the importance of the encapsulation (Figure 4A). For this reason, we have focused our attention on **DSPE-PEG-Biotin@2-O-IrAn**. Using the non-natural abundancy of Ir, the biodistribution of the nanoparticles within all major organs (i.e., heart, liver, spleen, kidney, lung) as well as in the tumor was determined by ICP-MS. While the majority of **DSPE-PEG-Biotin@2-O-IrAn** was found inside the liver, as observed for the vast majority of nanoparticle formulations, a significant amount was also found inside the tumor tissue. The maximal accumulation of the nanoparticles inside the tumor was reached 6 h after injection (Figure 4B). As a complementary technique, the accumulation was further studied time-dependently by an *in vivo* imaging system, which confirmed the biodistribution within the different organs as well as the tumor tissue (Figure 4D).

***In Vivo* Therapeutic Studies.** To study the therapeutic efficiency of **DSPE-PEG-Biotin@2-O-IrAn**, A549 tumor-bearing mice were injected with saline (group I/IV), cisplatin (group II/V) as a reference for clinically approved chemotherapeutic drugs and **DSPE-PEG-Biotin@2-O-IrAn** (group III/VI). 6 h after the intravenous injection, the mice were either kept in the dark or exposed to a two-photon irradiation by a 750 nm femtosecond pulsed laser (50 mW, 300 s). The tumor volume and body weight of each mouse was recorded every two days for two weeks. Promisingly, all mice behave normally without any signs of stress or discomfort and did not lose any weight, suggestive of the high biocompatibility of **DSPE-PEG-Biotin@2-O-IrAn** (Figure S40). While a single treatment with cisplatin showed some reduction of the tumor volume, two weeks after the treatment approximately 20-50% of the tumor volume remained and continued to grow exponentially. On the contrary, the tumors treated with **DSPE-PEG-Biotin@2-O-IrAn** were found to be nearly eradicated within a single procedure (Representative pictures of the mice/tumors: Figure S41/Figure 4E, Tumor growth inhibition curve: Figure 4C). This emphasizes the superior therapeutic effect of **DSPE-PEG-Biotin@2-O-IrAn** in comparison to the clinically approved PS Verteporfin. After the treatment, all major organs (i.e. heart, liver, spleen, lung, kidney, brain, intestine) as well as the tumor tissue were histologically examined by a hematoxylin-eosin stain. While no pathological alterations or injuries were observed for all organs (Figure S42), significant damage including chromatic agglutination and karyopyknosis was noticed in the tumor tissue (Figure 4E). As a complementary technique, the tumor tissue was analyzed by a terminal deoxynucleotidyl transferase dUTP nick end labeling (TUNEL) stain. While small amounts of green fluorescence signals, indicative for DNA strand breaks during apoptosis, for the treatment with cisplatin were observed, a significantly stronger signal for the treatment with **DSPE-PEG-Biotin@2-O-IrAn** was noticed, indicative of the strong therapeutic effect (Figure 4E). Overall, this study demonstrated the enormous potential of **DSPE-PEG-Biotin@2-O-IrAn** as encapsulated iridium(III) endoperoxide prodrug nanoparticles for synergistic photodynamic therapy/photoactivated chemotherapy.

Conclusion

In summary, in this article, a novel mitochondria-localized iridium(III) endoperoxide two-photon activated prodrug **2-O-IrAn** for synergistic hypoxic photodynamic and photoactivated chemotherapy is reported. While the photosensitizer is able to efficiently generate singlet oxygen under normoxic conditions, the compound is also able to release a highly cytotoxic Ir(III) complex, produce toxic singlet oxygen from the covalently bound oxygen molecule, and generate an alkoxy radical under hypoxic conditions. Due to this oxygen independent mechanism, the metal complex was found to be highly (photo-)toxic in hypoxic tumor cells and multicellular tumor spheroids in the nanomolar range. An in-depth investigation into the mechanism of action revealed that the compound primarily accumulates in the mitochondria, triggering loss of the mitochondrial membrane potential. To improve the pharmacological properties of the metal complex and provide a tumor selective uptake, the metal complex was encapsulated within a biotin functionalized phospholipid to form **DSPE-PEG-Biotin@2-O-IrAn** nanoparticles. The generated nanoparticles were found to nearly fully eradicate a tumor inside a mouse model upon two-photon irradiation in the NIR within a single treatment. This study presents, to the best of our knowledge, the first example of an iridium(III) endoperoxide prodrug for synergistic photodynamic therapy/photoactivated chemotherapy. The compound reported is one of the most efficient metal-based PDT PSs working under hypoxic conditions and that can be excited with 2P. This work opens up new avenues for the treatment of hypoxic tumors.

ASSOCIATED CONTENT

Supporting Information.

The Supporting Information is available free of charge at https://pubs.acs.org/doi/10.1021/jacs.1c09010.

Details on reagents, instruments, experimental sections including the synthesis procedures of iridium(III) complexes and DSPE-PEG-Biotin@2-O-IrAn, ROS generation, cellular uptake and localization, phosphorescence lifetime imaging microscopy, and (photo-)cytotoxicity in vitro and in vivo, as well as some additional supporting data.

AUTHOR INFORMATION

Corresponding Author

* gilles.gasser@chimieparistech.psl.eu (G.G.); ceschh@mail.sysu.edu.cn (H.C.)

ORCID

Shi Kuang: 0000-0003-3520-9499
Fangmian Wei: 0000-0003-3261-1677
Johannes Karges: 0000-0001-5258-0260
Kai Xiong: 0000-0002-8170-0273
Gilles Gasser: 0000-0002-4244-5097
Hui Chao: 0000-0003-4153-5303

Author Contributions

#Shi Kuang and Fangmian Wei contributed equally. The manuscript was written through contributions of all authors. All authors have given approval to the final version of the

manuscript.

ACKNOWLEDGMENT

This work was supported by the National Natural Science Foundation of China (Nos. 22120102002, 21778079), and the Science and Technology Innovation Program of Hunan Province of China (No. 2021RC5028).

REFERENCES

(1) Zhao, X.; Liu, J.; Fan, J.; Chao, H.; Peng, X. Recent progress in photosensitizers for overcoming the challenges of photodynamic therapy: from molecular design to application. *Chem. Soc. Rev.* **2021**, *50*, 4185-4219.

(2) Li, X.; Kwon, N.; Guo, T.; Liu, Z.; Yoon, J. Innovative Strategies for Hypoxic-Tumor Photodynamic Therapy. *Angew. Chem. Int. Ed.* **2018**, *57*, 11522-11531.

(3) Feng, G.; Zhang, G.-Q.; Ding, D. Design of superior phototheranostic agents guided by Jablonski diagrams. *Chem. Soc. Rev.* **2020**, *49*, 8179-8234.

(4) Sharma, A.; Arambula, J. F.; Koo, S.; Kumar, R.; Singh, H.; Sessler, J. L.; Kim, J. S. Hypoxia-targeted drug delivery. *Chem. Soc. Rev.* **2019**, *48*, 771-813.

(5) Karges, J., Clinical Development of Metal Complexes as Photosensitizers for Photodynamic Therapy of Cancer. *Angew. Chem. Int. Ed.* **2022,** *61*, e202112236.

(6) Cole, H. D.; Roque, J. A., 3rd; Lifshits, L. M.; Hodges, R.; Barrett, P. C.; Havrylyuk, D.; Heidary, D.; Ramasamy, E.; Cameron, C. G.; Glazer, E. C.; McFarland, S. A. Fine-Feature Modifications to Strained Ruthenium Complexes Radically Alter Their Hypoxic Anticancer Activity. *Photochem. Photobiol.* **2022**, doi: 10.1111/php.13395.

(7) Cole, H. D.; Roque, J. A.; Shi, G.; Lifshits, L. M.; Ramasamy, E.; Barrett, P. C.; Hodges, R. O.; Cameron, C. G.; McFarland, S. A. Anticancer Agent with Inexplicable Potency in Extreme Hypoxia: Characterizing a Light-Triggered Ruthenium Ubertoxin. *J. Am. Chem. Soc.* **2022**, doi: 10.1021/jacs.1c09010.

(8) Lameijer, L. N.; Ernst, D.; Hopkins, S. L.; Meijer, M. S.; Askes, S. H. C.; Le Devedec, S. E.; Bonnet, S. A Red-Light-Activated Ruthenium-Caged NAMPT Inhibitor Remains Phototoxic in Hypoxic Cancer Cells. *Angew. Chem. Int. Ed.* **2017,** *56*, 11549-11553.

(9) Lanquist, A. P.; Gupta, S.; Al-Afyouni, K. F.; Al-Afyouni, M.; Kodanko, J. J.; Turro, C., Trifluoromethyl substitution enhances photoinduced activity against breast cancer cells but reduces ligand exchange in Ru(ii) complex. *Chem. Sci.* **2021,** *12*, 12056-12067.

(10) Knoll, J. D.; Turro, C., Control and utilization of ruthenium and rhodium metal complex excited states for photoactivated cancer therapy. *Coord. Chem. Rev.* **2015,** *282-283*, 110-126.

(11) Havrylyuk, D.; Stevens, K.; Parkin, S.; Glazer, E. C. Toward Optimal Ru(II) Photocages: Balancing Photochemistry, Stability, and Biocompatibility Through Fine Tuning of Steric, Electronic, and Physiochemical Features. *Inorg. Chem.* **2020**, *59*, 1006-1013.

(12) Reynders, M.; Chaikuad, A.; Berger, B. T.; Bauer, K.; Koch, P.; Laufer, S.; Knapp, S.; Trauner, D., Controlling the Covalent Reactivity of a Kinase Inhibitor with Light. *Angew. Chem. Int. Ed.* **2021,** *60*, 20178-20183.

(13) Hansen, M. J.; Feringa, F. M.; Kobauri, P.; Szymanski, W.; Medema, R. H.; Feringa, B. L., Photoactivation of MDM2 Inhibitors: Controlling Protein-Protein Interaction with Light. *J. Am. Chem. Soc.* **2018,** *140*, 13136-13141.

(14) Cabrera, R.; Filevich, O.; Garcia-Acosta, B.; Athilingam, J.; Bender, K. J.; Poskanzer, K. E.; Etchenique, R., A Visible-Light-Sensitive Caged Serotonin. *ACS Chem. Neurosci.* **2017,** *8*, 1036-1042.

(15) Aubry, J. M.; Pierlot, C.; Rigaudy, J.; Schmidt, R. Reversible binding of oxygen to aromatic compounds. *Acc. Chem. Res.* **2003**, *36*, 668-675.

(16) He, Y. Q.; Fudickar, W.; Tang, J. H.; Wang, H.; Li, X.; Han, J.; Wang, Z.; Liu, M.; Zhong, Y. W.; Linker, T.; Stang, P. J., Capture and Release of Singlet Oxygen in Coordination-Driven Self-Assembled Organoplatinum(II) Metallacycles. *J. Am. Chem. Soc.* **2020,** *142* (5), 2601-2608.

(17) Schmidt, R.; Brauer, H. D. Comparison of the photochemical and thermal rearrangement reaction of endoperoxides. *J. Photochem.* **1986**, *34*, 1-12.

(18) Filatov, M. A.; Senge, M. O. Molecular devices based on reversible singlet oxygen binding in optical and photomedical applications. *Mol. Syst. Des. Eng.* **2016**, *1*, 258-272.

(19) Song, B.; Wang, G.; Tan, M.; Yuan, J., A europium(III) complex as an efficient singlet oxygen luminescence probe. *J. Am. Chem. Soc.* **2006**, *128*, 13442-13450.

(20) Ma, H.; Wang, X.; Song, B.; Wang, L.; Tang, Z.; Luo, T.; Yuan, J., Extending the excitation wavelength from UV to visible light for a europium complex-based mitochondria targetable luminescent probe for singlet oxygen. *Dalton Trans.* **2018**, *47*, 12852-12857.

(21) Zou, J.; Li, L.; Zhu, J.; Li, X.; Yang, Z.; Huang, W.; Chen, X. Singlet Oxygen "Afterglow" Therapy with NIR-II Fluorescent Molecules. *Adv. Mater.* **2021,** *33*, e2103627.

(22) Xie, B.-R.; Li, C.-X.; Yu, Y.; Zeng, J.-Y.; Zhang, M.-K.; Wang, X.-S.; Zeng, X.; Zhang, X.-Z. A Singlet Oxygen Reservoir Based on Poly-Pyridone and Porphyrin Nanoscale Metal–Organic Framework for Cancer Therapy. *CCS Chem.* **2020**, 1187-1202.

(23) Zou, J.; Zhu, J.; Yang, Z.; Li, L.; Fan, W.; He, L.; Tang, W.; Deng, L.; Mu, J.; Ma, Y.; Cheng, Y.; Huang, W.; Dong, X.; Chen, X. A Phototheranostic Strategy to Continuously Deliver Singlet Oxygen in the Dark and Hypoxic Tumor Microenvironment. *Angew. Chem. Int. Ed.* **2020,** *59*, 8833-8838.

(24) Turan, I. S.; Yildiz, D.; Turksoy, A.; Gunaydin, G.; Akkaya, E. U. A Bifunctional Photosensitizer for Enhanced Fractional Photodynamic Therapy: Singlet Oxygen Generation in the Presence and Absence of Light. *Angew. Chem. Int. Ed.* **2016**, *55*, 2875-2878.

(25) Kolemen, S.; Ozdemir, T.; Lee, D.; Kim, G. M.; Karatas, T.; Yoon, J.; Akkaya, E. U. Remote-Controlled Release of Singlet Oxygen by the Plasmonic Heating of Endoperoxide-Modified Gold Nanorods: Towards a Paradigm Change in Photodynamic Therapy. *Angew. Chem. Int. Ed.* **2016**, *55*, 3606-3610.

(26) Lai, H.; Yan, J.; Liu, S.; Yang, Q.; Xing, F.; Xiao, P. Peripheral RAFT Polymerization on a Covalent Organic Polymer with Enhanced Aqueous Compatibility for Controlled Generation of Singlet Oxygen. *Angew. Chem. Int. Ed.* **2020**, *59*, 10431-10435.

(27) Zeng, J. Y.; Wang, X. S.; Qi, Y. D.; Yu, Y.; Zeng, X.; Zhang, X. Z. Structural Transformation in Metal-Organic Frameworks for Reversible Binding of Oxygen. *Angew. Chem. Int. Ed.* **2019**, *58*, 5692-5696.

(28) Yuan, Z.; Yu, S.; Cao, F.; Mao, Z.; Gao, C.; Ling, J. Near-infrared light triggered photothermal and photodynamic therapy with an oxygen-shuttle endoperoxide of anthracene against tumor hypoxia. *Polym. Chem.* **2018**, *9*, 2124-2133.

(29) Fudickar, W.; Linker, T. Release of Singlet Oxygen from Aromatic Endoperoxides by Chemical Triggers. *Angew. Chem. Int. Ed.* **2018**, *57*, 12971-12975.

(30) Filatov, M. A.; Karuthedath, S.; Polestshuk, P. M.; Savoie, H.; Flanagan, K. J.; Sy, C.; Sitte, E.; Telitchko, M.; Laquai, F.; Boyle, R. W.; Senge, M. O. Generation of Triplet Excited States via Photoinduced Electron Transfer in meso-anthra-BODIPY: Fluorogenic Response toward Singlet Oxygen in Solution and in Vitro. *J. Am. Chem. Soc.* **2017**, *139*, 6282-6285.

(31) Callaghan, S.; Filatov, M. A.; Savoie, H.; Boyle, R. W.; Senge, M. O. In vitro cytotoxicity of a library of BODIPY-anthracene and -pyrene dyads for application in photodynamic therapy. *Photochem. Photobiol. Sci.* **2019**, *18*, 495-504.

(32) Jin, C.; Li, G.; Wu, X.; Liu, J.; Wu, W.; Chen, Y.; Sasaki, T.; Chao, H.; Zhang, Y. Robust Packing of a Self-Assembling Iridium Complex via Endocytic Trafficking for Long-Term Lysosome Tracking. *Angew. Chem. Int. Ed.* **2021,** *60*, 7597-7601.

(33) Chen, M. H.; Zheng, Y.; Cai, X. J.; Zhang, H.; Wang, F. X.; Tan, C. P.; Chen, W. H.; Ji, L. N.; Mao, Z. W. Inhibition of autophagic flux by cyclometalated iridium(iii) complexes through anion transportation. *Chem. Sci.* **2019,** *10*, 3315-3323.

(34) Kuang, S.; Liao, X.; Zhang, X.; Rees, T. W.; Guan, R.; Xiong, K.; Chen, Y.; Ji, L.; Chao, H. FerriIridium: A Lysosome-Targeting Iron(III)-Activated Iridium(III) Prodrug for Chemotherapy in Gastric Cancer Cells. *Angew. Chem. Int. Ed.* **2020,** *59*, 3315-3321.

(35) Wang, L.; Guan, R.; Xie, L.; Liao, X.; Xiong, K.; Rees, T. W.; Chen, Y.; Ji, L.; Chao, H. An ER-Targeting Iridium(III) Complex That Induces Immunogenic Cell Death in Non-Small-Cell Lung Cancer. *Angew. Chem. Int. Ed.* **2021,** *60*, 4657-4665.

(36) You, Y.; Nam, W. Photofunctional triplet excited states of cyclometalated Ir(III) complexes: beyond electroluminescence. *Chem. Soc. Rev.* **2012,** *41*, 7061-84.

(37) Zamora, A.; Vigueras, G.; Rodríguez, V.; Santana, M. D.; Ruiz, J. Cyclometalated iridium(III) luminescent complexes in therapy and phototherapy. *Coord. Chem. Rev.* **2018,** *360*, 34-76.

(38) Kuang, S.; Sun, L.; Zhang, X.; Liao, X.; Rees, T. W.; Zeng, L.; Chen, Y.; Zhang, X.; Ji, L.; Chao, H. A Mitochondrion-Localized Two-Photon Photosensitizer Generating Carbon Radicals Against Hypoxic Tumors. *Angew. Chem. Int. Ed.* **2020,** *59*, 20697-20703.

(39) Li, X.; Wu, J.; Wang, L.; He, C.; Chen, L.; Jiao, Y.; Duan, C. Mitochondrial-DNA-Targeted Ir-III-Containing Metallohelices with Tunable Photodynamic Therapy Efficacy in Cancer Cells. *Angew. Chem. Int. Ed.* **2020,** *59*, 6420-6427.

(40) Yuan, H.; Han, Z.; Chen, Y.; Qi, F.; Fang, H.; Guo, Z.; Zhang, S.; He, W. Ferroptosis Photoinduced by New Cyclometalated Iridium(III) Complexes and Its Synergism with Apoptosis in Tumor Cell Inhibition. *Angew. Chem. Int. Ed.* **2021,** *60*, 8174-8181.

(41) Qiu, K. Q.; Chen, Y.; Rees, T. W.; Ji, L. N.; Chao, H. Organelle-targeting metal complexes: From molecular design to bio-applications. *Coord. Chem. Rev.* **2019,** *378*, 66-86.

(42) Liu, J. P.; Zhang, C.; Rees, T. W.; Ke, L. B.; Ji, L. N.; Chao, H. Harnessing ruthenium(II) as photodynamic agents: Encouraging advances in cancer therapy. *Coord. Chem. Rev.* **2018,** *363*, 17-28.

(43) Guo, S.; Han, M.; Chen, R.; Zhuang, Y.; Zou, L.; Liu, S.; Huang, W.; Zhao, Q. Mitochondria-localized iridium(III) complexes with anthraquinone groups as effective photosensitizers for photodynamic therapy under hypoxia. *Sci. China: Chem.* **2019,** *62*, 1639-1648.

(44) Sullivan, L. B.; Chandel, N. S. Mitochondrial reactive oxygen species and cancer. *Cancer Metab.* **2014**, *2*, 17.

(45) Zong, W. X.; Rabinowitz, J. D.; White, E. Mitochondria and Cancer. *Mol. Cell.* **2016,** *61*, 667-676.

(46) Singh, K. K.; Kulawiec, M.; Still, I.; Desouki, M. M.; Geradts, J.; Matsui, S. Inter-genomic cross talk between mitochondria and the nucleus plays an important role in tumorigenesis. *Gene* **2005,** *354*, 140-146.

(47) Bugaj, A. M. Targeted photodynamic therapy-a promising strategy of tumor treatment. *Photochem. Photobiol. Sci.* **2011**, *10*, 1097-1109.

(48) Jung, H. S.; Han, J.; Shi, H.; Koo, S.; Singh, H.; Kim, H. J.; Sessler, J. L.; Lee, J. Y.; Kim, J. H.; Kim, J. S., Overcoming the Limits of Hypoxia in Photodynamic Therapy: A Carbonic Anhydrase IX-Targeted Approach. *J. Am. Chem. Soc.* **2017,** *139*, 7595-7602.

(49) Suzuki, S.; Tanaka, T.; Poyurovsky, M. V.; Nagano, H.; Mayama, T.; Ohkubo, S.; Lokshin, M.; Hosokawa, H.; Nakayama, T.; Suzuki, Y.; Sugano, S.; Sato, E.; Nagao, T.; Yokote, K.; Tatsuno, I.; Prives, C. Phosphate-activated glutaminase (GLS2), a p53-inducible regulator of glutamine metabolism and reactive oxygen species. *Proc. Natl. Acad. Sci. U. S. A.* **2010**, *107*, 7461-7466.

(50) Gogvadze, V.; Orrenius, S.; Zhivotovsky, B. Mitochondria in cancer cells: what is so special about them? *Trends Cell Biol.* **2008,** *18*, 165-173.

(51) Moreno-Sanchez, R.; Rodriguez-Enriquez, S.; Marin-Hernandez, A.; Saavedra, E. Energy metabolism in tumor cells. *FEBS J.* **2007**, *274*, 1393-1418.

(52) Lv, W.; Zhang, Z.; Zhang, K. Y.; Yang, H.; Liu, S.; Xu, A.; Guo, S.; Zhao, Q.; Huang, W. A Mitochondria-Targeted Photosensitizer Showing Improved Photodynamic Therapy Effects Under Hypoxia. *Angew. Chem. Int. Ed.* **2016**, *55*, 9947-9951.

(53) Heinemann, F.; Karges, J.; Gasser, G. Critical Overview of the Use of Ru(II) Polypyridyl Complexes as Photosensitizers in One-Photon and Two-Photon Photodynamic Therapy. *Acc. Chem. Res.* **2017**, *50*, 2727-2736.

(54) Aksakal, N. E.; Ecik, E. T.; Kazan, H. H.; Ciftci, G. Y.; Yuksel, F., Novel ruthenium(II) and iridium(III) BODIPY dyes: insights into their application in photodynamic therapy in vitro. *Photochem. Photobiol. Sci.* **2019,** *18* (8), 2012-2022.

(55) Zhao, J.; Yan, K.; Xu, G.; Liu, X.; Zhao, Q.; Xu, C.; Gou, S., An Iridium (III) Complex Bearing a Donor–Acceptor–Donor Type Ligand for NIR-Triggered Dual Phototherapy. *Adv. Funct. Mater.* **2020,** *31* (11), 2008325.

(56) Novohradsky, V.; Rovira, A.; Hally, C.; Galindo, A.; Vigueras, G.; Gandioso, A.; Svitelova, M.; Bresoli-Obach, R.; Kostrhunova, H.; Markova, L.; Kasparkova, J.; Nonell, S.; Ruiz, J.; Brabec, V.; Marchan, V., Towards Novel Photodynamic Anticancer Agents Generating Superoxide Anion Radicals: A Cyclometalated Ir(III) Complex Conjugated to a Far-Red Emitting Coumarin. *Angew. Chem. Int. Ed.* **2019,** *58* (19), 6311-6315.

(57) Huang, Z., A review of progress in clinical photodynamic therapy. *Technol. Cancer Res. Treat.* **2005,** *4*, 283-293.

(58) Zeitouni, N. Photodynamic therapy for nonmelanoma skin cancersCurrent review and update. *Mol. Immunol.* **2003**, *39*, 1133-1136.

(59) Bredell, M. G.; Besic, E.; Maake, C.; Walt, H. The application and challenges of clinical PD-PDT in the head and neck region: a short review. *J. Photochem. Photobiol. B* **2010**, *101*, 185-190.

(60) Juvekar, V.; Lim, C. S.; Lee, D. J.; Park, S. J.; Song, G. O.; Kang, H.; Kim, H. M. An azo dye for photodynamic therapy that is activated selectively by two-photon excitation. *Chem. Sci.* **2020**, *12*, 427-434.

(61) Raza, A.; Archer, S. A.; Fairbanks, S. D.; Smitten, K. L.; Botchway, S. W.; Thomas, J. A.; MacNeil, S.; Haycock, J. W. A Dinuclear Ruthenium(II) Complex Excited by Near-Infrared Light through Two-Photon Absorption Induces Phototoxicity Deep within Hypoxic Regions of Melanoma Cancer Spheroids. *J. Am. Chem. Soc.* **2020**, *142*, 4639-4647.

(62) Huang, H.; Yu, B.; Zhang, P.; Huang, J.; Chen, Y.; Gasser, G.; Ji, L.; Chao, H. Highly Charged Ruthenium(II) Polypyridyl Complexes as Lysosome-Localized Photosensitizers for Two-Photon Photodynamic Therapy. *Angew. Chem. Int. Ed.* **2015,** *54*, 14049-14052.

(63) Zhou, Z.; Liu, J.; Rees, T. W.; Wang, H.; Li, X.; Chao, H.; Stang, P. J. Heterometallic Ru-Pt metallacycle for two-photon photodynamic therapy. *Proc. Natl. Acad. Sci. U. S. A.* **2018**, *115*, 5664-5669.

(64) Freyer, W.; Stiel, H.; Hild, M.; Teuchner, K.; Leupold, D. One- and Two-Photon-Induced Photochemistry of Modified Palladium Porphyrazines Involving Molecular Oxygen. *Photochem. Photobiol.* **1997**, *66*, 596-604.

(65) Zhang, J.; Liu, D.; Liu, S.; Ge, Y.; Lan, Y.; Chen, Y. Visible-Light-Induced Alkoxyl Radicals Enable alpha-C(sp(3))-H Bond Allylation. *iScience* **2020**, *23*, 100755.

(66) Lee, S. H.; Oe, T.; Blair, I. A. Vitamin C-induced decomposition of lipid hydroperoxides to endogenous genotoxins. *Science* **2001**, *292*, 2083-2086.

(67) Hao, L.; Li, Z. W.; Zhang, D. Y.; He, L.; Liu, W.; Yang, J.; Tan, C. P.; Ji, L. N.; Mao, Z. W. Monitoring mitochondrial viscosity with anticancer phosphorescent Ir(iii) complexes via two-photon lifetime imaging. *Chem. Sci.* **2019**, *10*, 1285-1293.

(68) Ma, H.; Song, B.; Wang, Y.; Cong, D.; Jiang, Y.; Yuan, J. Dual-emissive nanoarchitecture of lanthanide-complex-modified silica particles for in vivo ratiometric time-gated luminescence imaging of hypochlorous acid. *Chem. Sci.* **2017**, *8*, 150-159.

(69) Chen, H.; Tian, J.; He, W.; Guo, Z. H2O2-activatable and O2-evolving nanoparticles for highly efficient and selective photodynamic therapy against hypoxic tumor cells. *J. Am. Chem. Soc.* **2015**, *137*, 1539-1547.

(70) Shen, J. C.; Rees, T. W.; Ji, L. N.; Chao, H. Recent advances in ruthenium(II) and iridium(III) complexes containing nanosystems

for cancer treatment and bioimaging. *Coord. Chem. Rev.* **2021**, *443,* 214016.

(71) Karges, J.; Li, J.; Zeng, L.; Chao, H.; Gasser, G. Polymeric Encapsulation of a Ruthenium Polypyridine Complex for Tumor Targeted One- and Two-Photon Photodynamic Therapy. *ACS Appl. Mater. Interfaces* **2020**, *12*, 54433-54444.